Optimizing Material Use in Blade Design by Improving Failure Prediction Methodology and Introducing Damage Tolerant Concepts in FRP Composites

A. E. Antoniou, T. P. Philippidis*
Dept. of Mechanical Engineering & Aeronautics
University of Patras, P. O. Box 1401, Patras 265 04, Greece

Abstract:

Preliminary results are presented in this work, concerning the validation of a reliable FEM tool under development, featuring damage tolerant concepts, to enhance design capabilities and optimize material use in large composite structures. User defined material constitutive equations concerning anisotropic non-linearity and material stiffness degradation as a result of damage accumulation, are implemented to model inherent damage tolerance of Fiber Reinforced Plastic (FRP) materials. Besides popular anisotropic failure conditions included in commercial FE codes, criteria that distinguish between different failure modes, e.g. Puck, are implemented and their performance is assessed.
Keywords: Damage tolerance, failure criteria, FRP composites.

1 Introduction

State-of-the-art design calculations for rotor blades, according to International Standards as well as widely accepted practices on mechanics of composites, consider FRP materials as linear up to failure and are in essence of "safe life" type in the sense no damage is allowed in the structure under the extreme static or fatigue loading cases. Damage in only one layer, either matrix cracking or fiber breakage is considered as the design limit condition. This corresponds to what is better known as state of "First Ply Failure" (FPF) for composites. However fiber reinforced composites accumulate damage, resisting in total failure through stress redistribution mechanisms. Though, after that load level, usually the composite laminates, depending also on the stacking sequence, exhibit substantial load bearing capacity up to ultimate failure, "Last Ply Failure" (LPF), which remains unexploited. Germanischer Lloyd since its 2004 edition has adopted the implementation of stress cases in which limited material damage, mainly in the form of matrix cracks that run parallel to the fibres, is still acceptable. Although not requested by design regulations at present, to correctly implement such type of analyses in blade design one needs to fully characterize material elastic properties, highly non-linear in some aspects, use failure criteria accounting for the various failure modes encountered in FRP composites and utilize the appropriate stiffness and strength degradation scenarios.

Numerous anisotropic failure criteria have been proposed up to now for FRP composites. They can be broadly distinguished to *macroscopic* such as the quadratic form of failure tensor polynomial, better known as Tsai-Wu criterion [1] and those that discriminate between different failure modes, a concept introduced by Z. Hashin [2]. He has first presented a phenomenological failure criterion with separate equations to describe different modes of damage. Theoretical base for this assumption was Mohr's hypothesis for brittle materials that fracture is exclusively created by stresses applied on the fracture plane. Puck et al [3] have established a more generalized set of criteria, providing a number of user defined parameters enhancing modeling flexibility. Comparison between several failure criteria and a large discussion on their efficiency in correctly predicting failure, took place in the 'World Wide Failure Exercise' [4].

After failure onset, damage progress scenarios due to strength and stiffness degradation, are of vital importance in predicting ultimate load at final rupture, LPF. Chang et al [5] proposed a progressive damage analysis implementing a failure criterion that distinguishes between different failure modes. An analytical expression was used to model the non-linear

* To whom correspondence should be addressed: tel/fax: +30-2610-997235, e-mail:philippidis@mech.upatras.gr

shear stress-strain behavior. An abrupt elastic degradation rule was used, reducing the mechanical properties, depending on the predicted failure mode. Lin et al [6] have suggested a linear degradation rule only for the transverse, to the fiber direction, elastic modulus. Puck et al [7], [8] have introduced an efficient albeit more complex progressive damage rule for transverse elastic, shear moduli and Poisson ratios.

In the present work, non-linear material properties for a Glass/Epoxy system are characterized in detail in the course of a comprehensive experimental program that consists amongst others of static and cyclic tests in uni- and multi-directional laminates on- and off-axis.

A detailed investigation of failure predictions using the Puck criteria is presented in this paper suggesting best practice rules for this type of Glass/Epoxy system. Non-linear material behavior, failure criteria and progressive damage scenarios are implemented in the commercial finite element code ANSYS v.8.1, in a shell element, but can be also easily transferred to any other FE platform, prompting for damage tolerant design of wind turbine rotor blades. A layer by layer plane stress analysis is carried out in a variety of laminated coupons of different stacking sequences that are statically loaded to failure. Either tensile or compressive tests are performed and detailed experimental data in the form of stress-strain curves are compared with FEM results. The agreement between the two sets of data is remarkably good.

2 Material Performance

2.1 Material Properties

Mechanical properties are obtained through a series of coupon tests. A standard specimen geometry is adopted for all tests either static or fatigue for the unidirectional material [9]. It is of rectangular shape with nominal dimensions of 145mm long, 25mm wide and 35mm gauge length between tabs. Number of layers, hence thickness, varies depending on the property under investigation. Unidirectional coupons loaded in the fiber direction are nominally 3.52mm thick while those loaded transversely to the fibers are 6.16mm. The corresponding specimen for multidirectional material lay up, composed of layers at 0, +45 and -45 degrees, is 150mm long, 25mm wide and there is a 40mm gauge length between tabs. Nominal thickness is considered to be 6.57mm. For shear modulus and strength evaluation, ISO-14129 standard coupon is used. Strain measurements are conducted on both coupon faces, in the middle of the gauge length and an average is considered as the experimentally obtained value.

However as previously stated, FRP composites with organic matrix, exhibit highly non-linear stress-strain behavior, especially in shear and compression transversely to the fibers, see Fig.1, 2. Hence, non-Hookean material behaviour is anticipated:

$$\sigma_i = C_{ij}(\sigma_i)\varepsilon_j \,, i, j = 1,\ldots,6 \qquad (1)$$

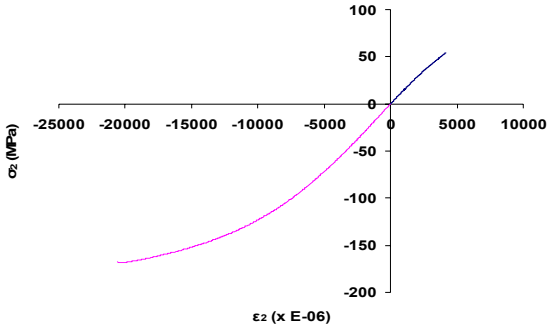

Figure 1: Tension-compression in the transverse to the fiber direction for UD Glass/Epoxy

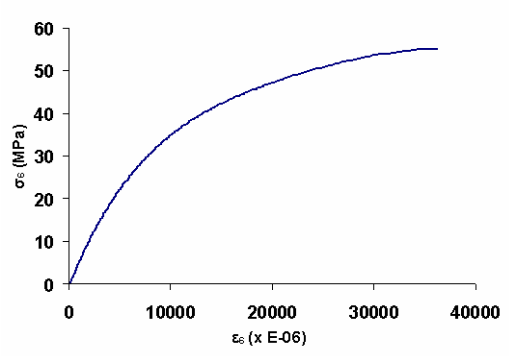

Figure 2: Shear stress-strain behaviour of UD material.

Tangential elasticity moduli are used in a sense of piecewise linear regions that compose the full non-linear stress-strain curve. The assigned modulus value is selected with respect to the existing stress level, e.g. $E_2=f(\sigma_2)$ etc.

In the fiber direction, non-linearity is not so evident either in tension or compression, although it exists and it is taken into account in the FEM model.

2.2 Failure Onset

Material damage initiates and propagates as the load increases. The failure criterion of Puck is implemented to assess the magnitude of damage and to distinguish between different failure modes [3], [8]. Fiber failure is estimated in fact by means of the maximum stress criterion either in tension or compression:

Fiber failure in tension, $\sigma_1>0$:

$$\frac{\sigma_1}{X_T} \geq 1 \qquad (2)$$

Fiber failure in compression, $\sigma_1<0$:

$$\left|\frac{\sigma_1}{X_C}\right| \geq 1 \qquad (3)$$

σ_1 is the stress in the fibers direction and X_T, X_C are the ultimate tensile (UTS) and compressive (UCS) stresses of the unidirectional layer. It is noted that UCS is taken from tests using coupons of ISO geometry, since the standard coupon geometry previously mentioned, suffered from buckling. The value of the failure criterion for the fibers is referred to as $f_{E(FF)}$.

Matrix failure transverse to the fibers due to tensile stresses, $\sigma_2>0$:

$$\sqrt{\left(\frac{\sigma_6}{S}\right)^2+\left(1-p^{(+)}_{\perp\parallel}\frac{Y_T}{S}\right)^2\left(\frac{\sigma_2}{Y_T}\right)^2}+p^{(+)}_{\perp\parallel}\frac{\sigma_2}{S}+\left(\frac{\sigma_1}{\sigma_{1D}}\right)^6 \geq 1 \qquad (4)$$

This type of failure is denoted as mode A, see Fig.3, and results to cracks that open transversely to the applied load, parallel to the fibers. In the failure condition, σ_6 is the shear stress developed in the (1-2) principal plane of the layer. S is the in-plane shear strength, σ_2 is the normal stress transverse to the fibers and Y_T its respective ultimate. The term σ_1/σ_{1D} takes into account the matrix damage that occurs after the fiber breakage. For simplification, this ratio is supposed to be 0.9 of the fiber failure effort [3]. It is raised in the 6th power in order to affect the rupture condition only in high tensile loads. Parameter $p^{(+)}{}_{\perp\parallel}$ represents the slope of the failure locus (σ_2, σ_6) at $\sigma_2=0^+$. It is obtained with a fitting procedure on experimental data with positive normal stress ($\sigma_2\geq 0$). Puck et al [8] give guidelines for the determination of this parameter and some typical values for FRP materials. For the Glass/Epoxy material at hands, it is chosen equal to 0.3.

Matrix failure transverse to the fibers when compressive stresses are developed, $\sigma_2\leq 0$ and $0 \leq |\sigma_2 / \sigma_6| \leq R^A{}_{\perp\perp} / |\sigma_{6c}|$:

$$\frac{1}{S}\left(\sqrt{(\sigma_6^2)+(p^{(-)}_{\perp\parallel}\sigma_2)^2}+p^{(-)}_{\perp\parallel}\sigma_2\right)+\left(\frac{\sigma_1}{\sigma_{1D}}\right)^6 \geq 1 \qquad (5)$$

In that case cracks are formed parallel to the fibers, relatively closed when compared to those of mode A. The failure mode is denoted as B and the shear stresses σ_6 for failure onset are increased along with the magnitude of the compressive normal stress σ_2, see Fig.2. The parameter $p^{(-)}{}_{\perp\parallel}$ represents the slope of the failure locus (σ_2, σ_6) at $\sigma_2=0^-$. It is derived from experimental data with negative normal stress ($\sigma_2\leq 0$). Puck et al [8] suggest again some typical values for FRP materials. In the present work it is chosen equal to 0.25. Parameter $R^A{}_{\perp\perp}$ stands for the ultimate transverse shear strength and it is defined analytically by Puck et al [8].

Further increase of the compressive transverse stress σ_2 leads to an explosive matrix failure type that is called mode C, $\sigma_2\leq 0$ and $0 \leq |\sigma_6 / \sigma_2| \leq |\sigma_{6c}| / R^A{}_{\perp\perp}$, see Fig.3:

$$\left[\left(\frac{\sigma_6}{2\left(1+p^{(-)}_{\perp\perp}\right)S}\right)^2+\left(\frac{\sigma_2}{Y_C}\right)^2\right]\left(\frac{Y_C}{(-\sigma_2)}\right)+\left(\frac{\sigma_1}{\sigma_{1D}}\right)^6 \geq 1 \qquad (6)$$

Damage occurs in a plane that is not perpendicular to the one defined by the in plane stresses. The parameter $p^{(-)}{}_{\perp\perp}$ represents the inclination of the failure locus (σ_2, σ_4) at $\sigma_2=0$. Since it is very difficult to perform such kind of experiments, Puck et al [8] suggests an empirical formula to estimate the slope. The term Y_C stands for the ultimate compressive stress transverse to the fibers direction. The value of the matrix failure criterion is referred to as stress exposure factor $f_{E(IFF)}$.

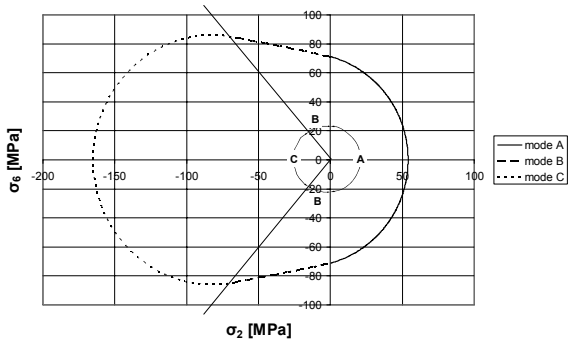

Figure 3: Failure locus in the (σ_2, σ_6) stress space, predicted with Puck failure criterion.

3 Damage Propagation

Stiffness degradation follows failure onset. Depending on the damage mode, different stiffness reduction policies are implemented. Since failure mode A results in matrix cracks that tend to open, it is supposed that no stresses normal to the crack or shear loads can be transferred. Hence transverse Young modulus E_2, shear modulus G_{12} and minor Poisson ratio v_{21} are degrading simultaneously. The degradation factor is chosen equal for all the properties. In damage modes B and C, matrix cracks developed during the loading, tend to close due to compressive stresses. However, a certain sliding movement of the crack faces relative to each other is expected to occur. Consequently a degradation factor is applied only in shear modulus value.

A progressive stiffness degradation model is adopted [7], according to which the degradation factor is given by:

$$\eta = \frac{1-\eta_r}{1+c(f_{E(IFF)}-1)^{\xi}} + \eta_r \qquad (7)$$

where c, ξ and η_r are model parameters defined by means of basic tests. The term η_r represents the remaining stiffness of the ply after damage accumulation reaches saturation level. Puck et al [7] have originally suggested typical values of c≈4 and ξ≈2, for FRP composites. However, this set of values has to be defined for any new material system. In the present work, the parameters as implemented in the FEM model were taken equal to c=18 and ξ=2. The term η_r depends on the loading case and was taken equal to 0.01 for mode A and 0.9 for modes B and C. Parameter selection was based on the optimal simulation of the results from tensile tests of $[\pm 45]_s$ and $[90]_7$ coupons.

When fiber breakage occurs, stiffness degrades by multiplying all engineering elastic constants by a factor, say 1E-05, but not set equal to zero, so as no further load can be carried from the ruptured material, avoiding simultaneously numerical convergence problems.

For the calculation of the degradation factor η, a back-and-forth virtual load step procedure is implemented in the FEM user routine. The stress exposure factor $f_{E(IFF)}$ for matrix cracking is calculated for each layer. If no failure is observed ($f_{E(IFF)}<1$) then η=1 and the solution continues with the next load step. Otherwise, if $f_{E(IFF)}=1$ the layer has reached its crack onset point. Depending on the failure mode, the values of the corresponding elasticity moduli and Poisson ratio are saved and kept frozen under different variable names for further virtual loading calculations. Applying a virtual load increase and using the elasticity properties before failure onset results in a non realistic stress distribution and to $f_{E(IFF)}$ values greater than unity. The difference $f_{E(IFF)}$ -1 increases with load and so it can be considered as a representative parameter of matrix crack accumulation. An unloading step follows recalculating stress and strains using the initial elasticity before damage propagation. Finally, a reloading step is performed with the degraded properties applied. Subsequently the solution continues to the next load step.

4 Model Implementation

Four different FEM models were implemented so as to account for differences in coupon geometry and lay-up:

a) unidirectional coupon having fibers parallel to the loading axis (1488 elements, 4 layers).
b) unidirectional coupon with fibers transversely to the loading direction (1488 elements, 7 layers).
c) multidirectional coupon (1488 elements, 14 layers).
d) [±45] coupon (2400 elements, 4 layers).

In all specimens node displacements and rotational degrees of freedom were constrained in one tab region while force is incrementally applied on the other tab area, see Fig.4. Load-step resolution is specified so as to simulate material non-linearity and to avoid numerical convergence problems.

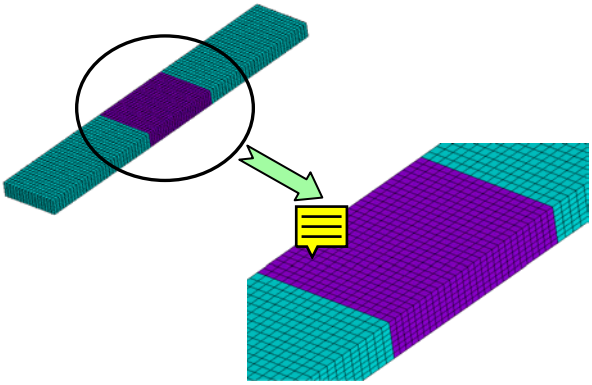

Figure 4: FEM model of a test coupon.

Analysis is done with ANSYS commercial FEM code. A 3-D shell element (SHELL181) implementing first order shear deformation theory (Mindlin-Reissner) was used. A user defined constitutive model [10] was implemented in a FORTRAN routine, compatible with the specific element. Material non-linear behaviour, failure criteria and progressive damage scenarios are incorporated in this routine which is compiled with ANSYS core code, resulting in a new ANSYS executable file. Using this procedure saves a lot of time when running the FEM code instead of programming the progressive damage concept with the APDL-ANSYS programming language. For the results presented in this work the most time consuming model has 2400 elements, 15000 dofs and needs up to one hour to be solved while using APDL based routines would need over 24 hours of computational time in the same processor.

5 FEM vs. Experimental Data

5.1 Tension of Glass/Epoxy $[\pm 45]_s$ coupon .

Material response in shear stress is highly non-linear. To validate model effectiveness in predicting such a performance, an ISO $[\pm 45]_s$ coupon, used for the material shear modulus determination, is modeled

under tensile loading. The FEM calculations seem to agree with experimental strain measurements in the axial (loading) and transverse directions, Fig.5, following the curve slope reduction and correctly also predicting coupon strength.

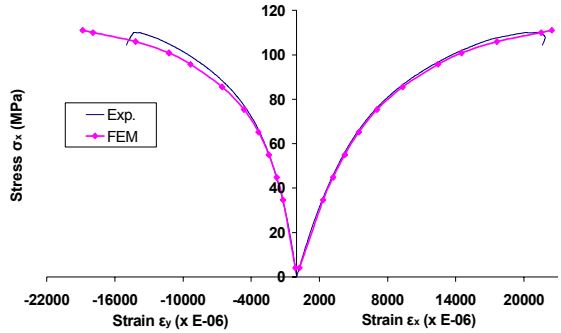

Figure 5: Stress-Strain behavior of a $[\pm 45]_s$ coupon.

Damage propagation map with load evolution is simulated in Fig. 6. Failure initiates in the region next to the right tabs while catastrophic separation is considered to occur when cracks are bridged trough the specimen width, in all plies, Fig. 6d.

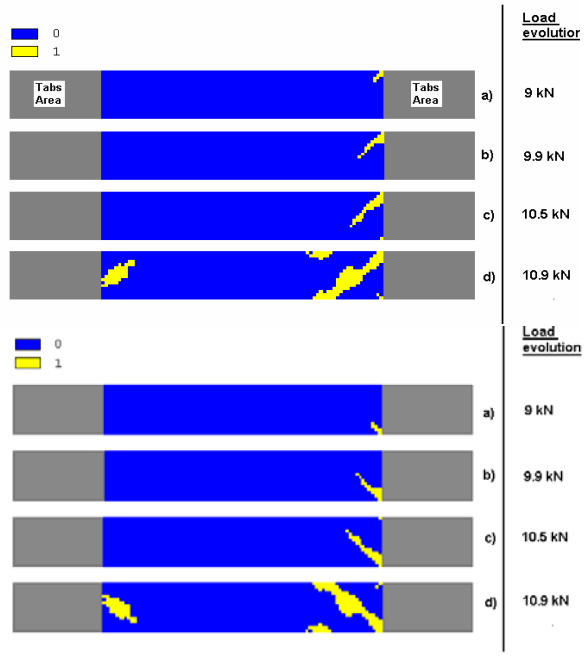

Figure 6: Predicted damage propagation in the 1st and 2nd layers of a $[\pm 45]_s$ coupon under tensile loading.

Area indicated with number 0 corresponds to intact material while region designated with number 1 highlights the damaged material failed under mode A. The prediction is fairly close to the observed experimental failure mode shown in Fig. 7.

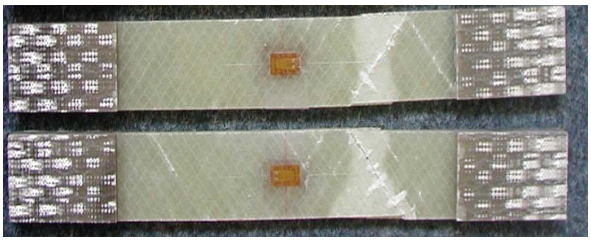

Figure 7: Upper & Lower faces of a failed $[\pm 45]_s$ coupon, under tensile loading.

5.2 Compression of a $[90]_7$ coupon (transverse to the fibers).

Loading is applied in the direction transverse to the fibers where matrix performance dominates. Material non-linear behavior is obvious, see Fig.1, especially in the compression quadrant. The FEM results for the 7 layer coupon are in excellent agreement with the experimental data, Fig. 8, while a satisfactory also prediction for the ultimate compressive stress is obtained.

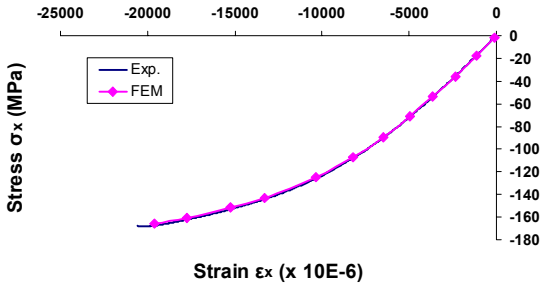

Figure 8: Stress-Strain behavior of a $[90]_7$ coupon in compression.

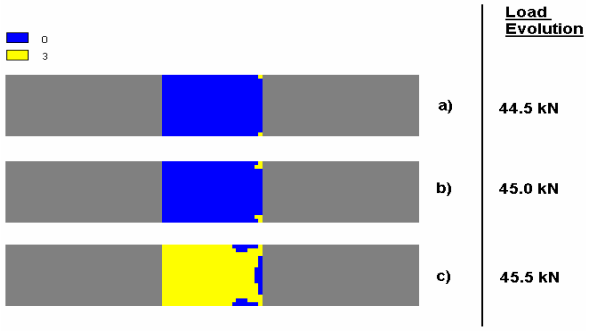

Figure 9: Predicted damage propagation in a $[90]_7$ coupon under compressive loading.

Failure initiates near the tabs region but this time failure occurs abruptly, in a sense of a 'Sudden Death'

manner, Fig. 9c. The cracks appearance leads almost immediately to a catastrophic failure of type C that is indicated by the region corresponding to number 3. No damage is present in area designated with number 0.

Although the 'Sudden Death' model matches well with the specimen experimental behavior, the damage pattern shown in Fig. 9c is not accurate as it can be seen by comparison with the photos of the failed coupon, Fig.10. This is due to the resolution of loading steps in the numerical calculations and the sudden failure occurrence for this type of geometry and loading. Failure maps of Fig.9 could be improved by augmenting substantially the number of load steps, increasing in parallel CPU time. This was not judged necessary since ultimate stress prediction was satisfactory. In addition, an excellent verification of the failure mode C, i.e. an oblique matrix crack with respect to the compressive load direction, predicted by the FEM model is provided by the lateral view of the failed coupon in Fig.10.

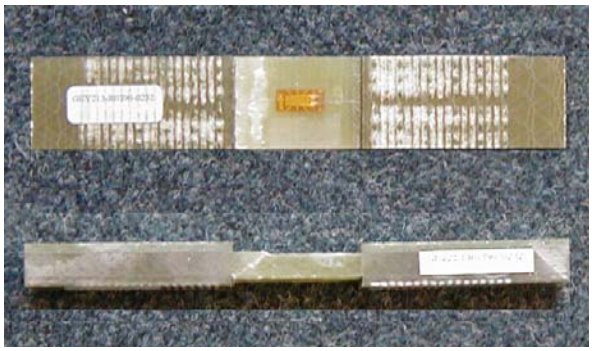

Figure 10: Front & Lateral side of a failed $[90]_7$ coupon in compression.

5.3 UniDirectional (UD) Glass/Epoxy coupon, $[0]_4$ under tension.

A tensile load case along the fibers is simulated for the 4 layer UD coupon. Axial and transverse strains on the specimen faces measured in the test compare well with FEM results, Fig. 11.

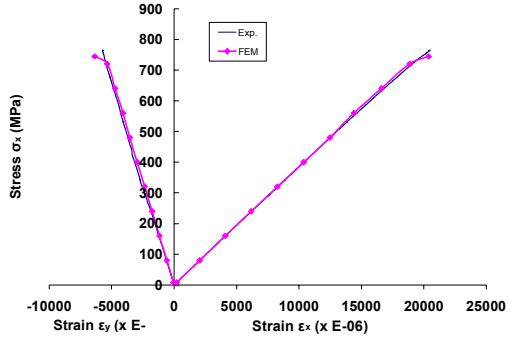

Figure 11: Stress-Strain behavior of a $[0]_4$ coupon in tension.

The UTS is derived by dividing the experimentally defined failure load with the specimen cross sectional area, assuming a homogeneous stress field in the gauge length area. This value is used in the maximum stress failure criterion as the allowable stress. From the numerical analysis it arises that the developed stresses in the middle of the coupon are smoothly distributed and are almost equal to the $\sigma_x=F_x/A$ ratio. F_x is the external imposed load and A is the specimen cross sectional area. This is shown in Fig.12 where for a specific external load, the developed stress field is presented. The stresses highlighted with blue color are in the range between 638-642 MPa while the externally imposed axial stress is 640 MPa. An even stress distribution would have resulted in a failure load prediction equal to the experimental. However a stress concentration region emerges near the coupon right tabs area, due to boundary constraints where higher stress values than in the middle of the specimen built up. Hence the composite fails earlier near the tabs area than in the rest of the material. That is the reason leading the FEM model in a relatively premature failure, i.e. predict a UTS of 740 instead of 770 MPa.

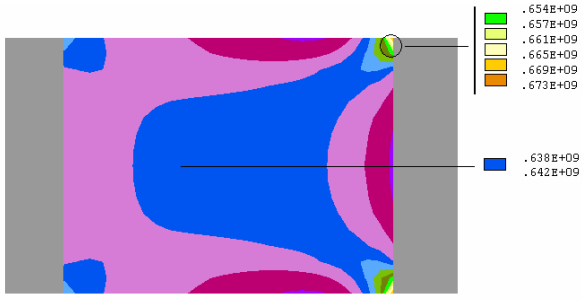

Figure 12: Normal axial stress distribution in the gauge area of a $[0]_4$ coupon in tension.

The numerical simulation predicts fiber breaks starting near tabs region that finally propagate along the specimen length, Fig.13. This result compares favorably with the experimental failure modes, Fig.14.

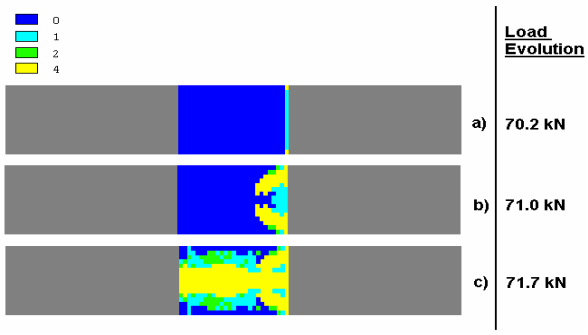

Figure 13: Predicted damage propagation in the UD $[0]_4$ coupon.

Area indicated with number 0 is the intact area while regions designated with numbers 1, 2, 3 have failed correspondingly under the three matrix failure modes A, B and C. The damage mode that dominates is the fiber fracture pointed out with yellow color and number 4.

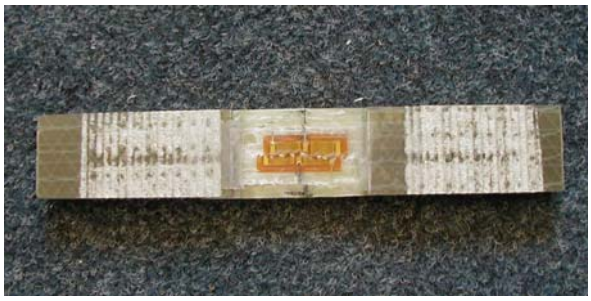

Figure 14: Failed $[0]_4$ coupon in tension.

5.4 Tension of an MD coupon along the fibers of the [0] layer.

The multidirectional coupon (MD), is composed of layers of UD [0] and stitched bi-directional [±45] fabric. This case is simulated so as to further evaluate the progressive damage concept on a more complex laminate. A comparison between numerical and test results is presented in fig. 15.

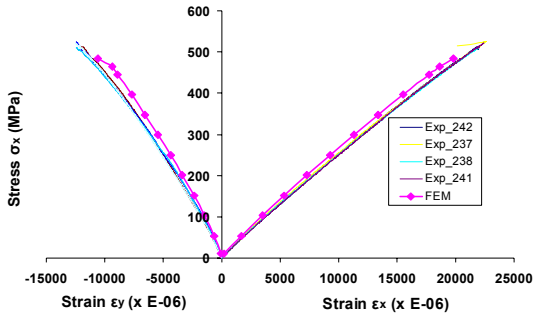

Figure 15: Stress-Strain behavior of an MD coupon in tension.

The FEM model predicts satisfactorily the material stress-strain curve although it behaves a little stiffer than the tested material and the calculated tensile strength is slightly lower than the experimental one. Premature failure is caused from stress concentration in the unidirectional [0] layers, near the tabs region. It is the same phenomenon that arises in the UD [0] coupon. Damage evolution in the upper unidirectional layer is presented in Fig. 16. Fiber breaks start near the tabs area. Sectional weakness leads to further fiber failure till the final rupture. All [0] layers fail simultaneously with the same failure modes approximately.

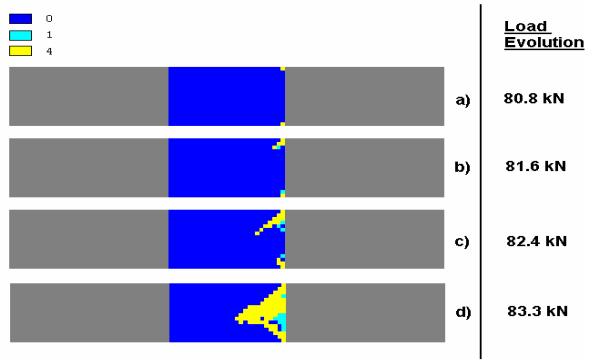

Figure 16: Damage evolution in the upper [0] ply of the MD coupon.

Well before [0] ply failure onset, damage initiates and propagates in [±45] layers. The failure mode is type A, hence tensile matrix cracks occur and accumulate through specimen width, Fig 17.

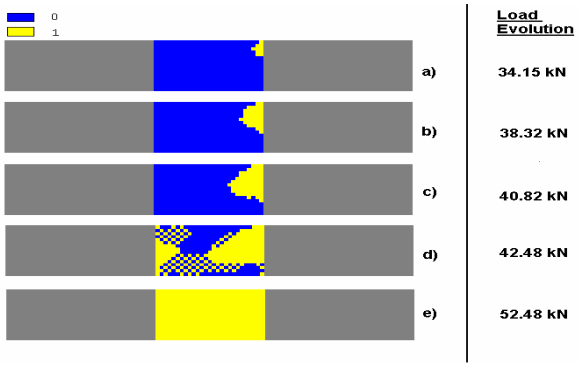

Figure 17: Damage evolution in the [45] layer of the MD coupon.

A direct comparison cannot be done between the simulated and the experimental failure mode for all layers, except the presence of extended damage on the upper [45] layer, Fig.18. Ultrasonic C-scan tests could enhance further assessment.

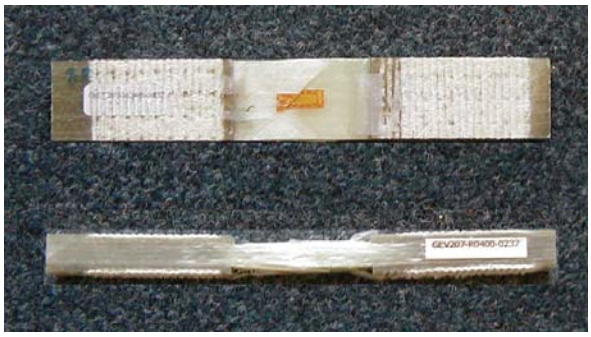

Figure 18: Failed MD coupon in tension.

Furthermore, coupon catastrophic failure occurs in the tab area and this is correctly predicted by the FEM model, see Fig.17.

5.5 Compression of an off-axis loaded, at 10°, MD coupon

To induce complex stress states in principal material coordinates, multidirectional specimens cut in various off-axis angles with respect to the MD [0] ply, are loaded either in tension or compression. The MD [10] coupon is cut at 10° and it is therefore composed of [55], [-35] and [10] layers. It is a highly anisotropic lay-up, unbalanced and non-symmetric leading to severe structural couplings. FEM results are in good agreement with the experimental data. The numerical model is less stiff but predicts the ultimate compressive stress with fine precision, Fig.19.

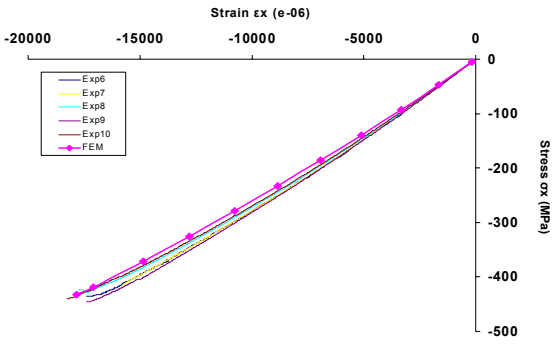

Figure 19: Stress-Strain behavior of an MD [10] coupon in compression.

Damage initiates and accumulates in the [10] plies as tensile matrix cracks of type A. After fiber compressive failure emanates from the tabs area, indicated with number 5, final rupture occurs in an abrupt way, Fig.20.

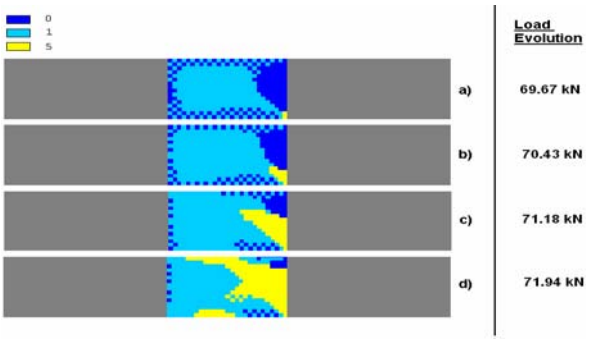

Figure 20: Damage evolution in the upper [10] layer of the MD coupon off-axis compressed.

Failure of the outer [55] ply, according to the numerical predictions happens suddenly. One load step before final rupture, the layer is not extensively damaged, Fig.21.

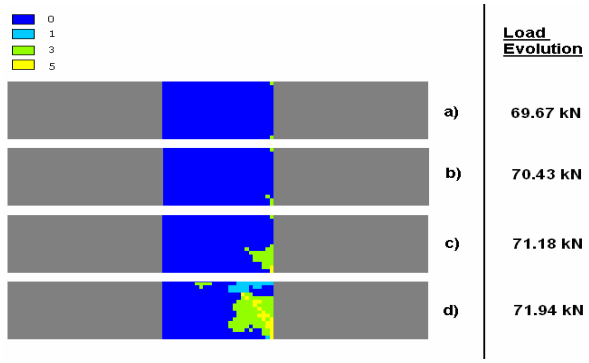

Figure21: Damage evolution in the outer [55] layer of the MD coupon

Examining the tested coupons surfaces, Fig.22, extended damage near the tabs region is noticed. This appearance is due to matrix cracking, which is predicted from the numerical calculations for the upper layer. Furthermore the FEM model predicts fairly well the location of the final failure crack, through the thickness, which is also near the same tab region, Fig.20.

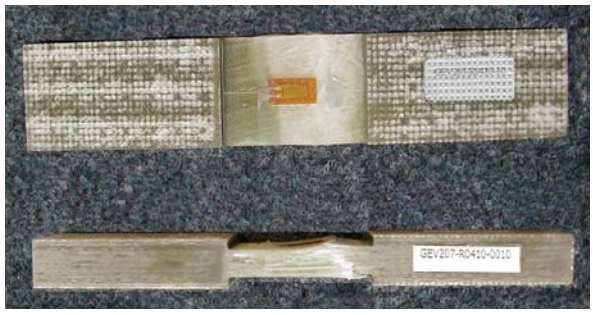

Figure 22: Failed MD coupon loaded off-axis in compression at 10°.

5.6 Tension of an off-axis loaded, at 60°, MD coupon.

The MD 60 specimen is cut at 60 degrees with respect to the [0] ply and it is composed of [15], [-85] and [60] plies. In these tests matrix non-linear performance dominates the coupon stress-strain behavior. The numerical simulation approaches well the material deformation up to the experimental failure point but it highly overestimates the ultimate load, Fig.23.

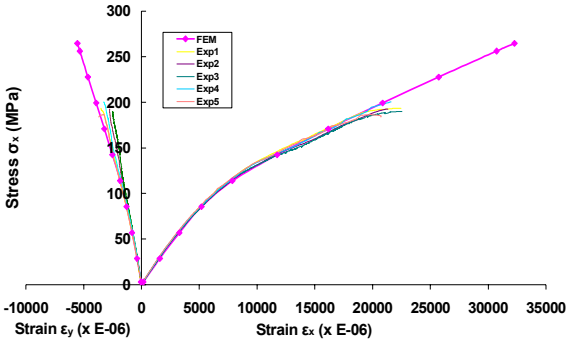

Figure 23: Stress-Strain behavior of an MD 60 coupon in tension.

Puck criterion with the specific set of inclination parameters, defined previously in section 3 of this work, does not effectively predict final failure under the particular stress field. Possibly, another parameter set could fit better these experimental data. This discrepancy is the most extreme met amongst all the simulated models.

According to the FEM calculations, the last ply that fails is the 15 degree lying on coupon surface. Prediction of damage propagation is presented in Fig.24. Final rupture is caused due to broad matrix cracking of type A that bridges the specimen width.

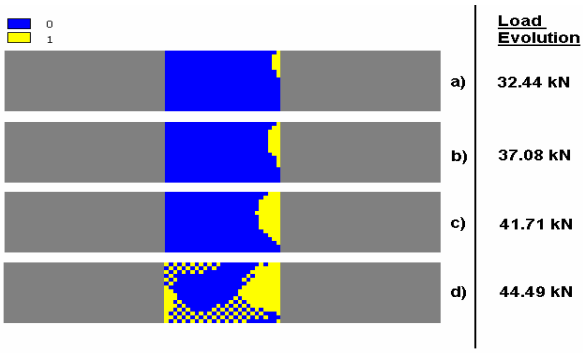

Figure 24: Damage evolution in the outer [15] ply of the MD 60 coupon.

The experimentally observed failure pattern is presented in Fig. 25, and it is not amenable to direct correlation with the numerical model.

Figure 25: Failed MD coupon loaded off-axis in tension at 60°.

6 Conclusions

In the present work, an anisotropic non-linear material constitutive model is implemented in a shell element of the ANSYS commercial FEM code by means of a user FORTRAN routine. Progressive damage concepts are employed to characterize the load carrying capacity of composite structures. Puck criterion, enhancing failure characterization by distinguishing between different damage modes, is implemented. In most cases the failure patterns can be directly compared with the experimentally observed, especially in the unidirectional and the $[\pm 45]_s$ coupons. In multidirectional specimens although the damage trend is approached, ultrasonic methods could highlight further similarities. Different stiffness degradation strategies are utilized depending on the predicted failure mode. The solution procedure is fast enough allowing simulations of large models in a reasonable computational time.

Material properties are fully characterized for the unidirectional layer in shear and either in tension or compression, parallel and transverse to the fibers direction. Given all deformation and ultimate stress data, numerical simulation of loading coupons of complex lamination is performed. The FEM model follows very well material stress-strain behavior and calculates the failure load with an error up to 5-6%. The only exception is the prediction made for the tensile test of the multidirectional coupon at 60° where although the material nonlinear deformation is predicted satisfactorily, the estimation of the failure load is optimistic by 34.5%. A different set of material failure parameters for the Puck criterion could possibly improve the numerical predictions.

7 Acknowledgements

Research funded in part by European Commission in the framework of the research programme “Reliable Optimal Use of Materials for Wind Turbine Rotor Blades” (OPTIMAT BLADES), contract No: ENK6-CT-2001-00552 and in part by the General Secretariat of Research and Technology (GSRT) of the Greek Ministry of Development, contract No. F.K. 6660.

8 References

[1].Tsai, S. W. and Wu, E. M., "A general theory of strength for anisotropic materials", *J. Compos. Mater.,* 1971, **5**, 58-80

[2].Hashin, Z., "Failure criteria for unidirectional fiber composites", *J. Appl. Mech.*, 1980, **47**, 329-334

[3].Puck, A., Schürmann, H., "Failure analysis of FRP laminates by means of physically based phenomenological models", *Compos. Sci. Tech.*, 1998, **58**, 1045-1067

[4].Hinton, M. J., Kaddour A. S. and Soden P. D., “A comparison of the predictive capabilities of current failure theories for composite laminates, judged against experimental evidence” *Compos. Sci.Tech.*, 2002, **62**, 1725-1797

[5].Chang, K., Liu, S. and Chang, F., "Damage tolerance of laminated composites containing an open hole and subjected to tensile loadings", *J. Compos. Mater.,* 1991, **25**, 274-301

[6]. Lin, W. and Hu, H., "Nonlinear analysis of fiber-reinforced composite laminates subjected to uniaxial tensile load", *J. Compos. Mater.,* 2002, **36**, 1429-1450

[7].Puck, A., Schürmann, H., "Failure analysis of FRP laminates by means of physically based phenomenological models", *Compos. Sci.Tech.*, 2002, **62**, 1633-1662

[8]. Puck, A., Kopp, J. and Knops, M., "Guidelines for the determination of the parameters in Puck’s action plane strength criterion", *Compos. Sci.Tech.*, 2002, **62**, 371-378

[9].Philippidis, T. P., Antoniou A. E., Assimakopoulou T. T., Passipoularidis V. A., “Static tests on the standard OB UD and MD off-axis coupons”, OB_TG2_R022_rev.000, report # 10254, OPTIMAT BLADES, 2005

[10]. Guide to ANSYS programmable features, ANSYS Release 6.1, 2002